

RESEARCH ARTICLE

Suspension Strategy of Maglev Vertical Axis Wind Turbine Based on Sliding Mode Adaptive Neural Network Predictive Control

YIXI CHEN, YANG ZHANG, AND BIN CAI

School of Engineering, Qufu Normal University, Rizhao 276826, China

Corresponding author: Bin Cai (bincai1027@qfnu.edu.cn)

This work was supported by the National Natural Science Foundation of China under Grant 61473170.

ABSTRACT The magnetic levitation system of the maglev vertical axis wind turbine is presented in this paper. The design and implementation of the magnetic levitation controller are discussed, and the nonlinear mathematical model of the magnetic levitation system is established. However, the magnetic levitation system is extremely susceptible to disturbance. To suppress the external disturbance and parameter perturbations, a sliding mode adaptive neural network predictive control method is presented, which is composed of the sliding mode control, an adaptive neural network and a model predictive control. The sufficient simulation and experimental results show that the proposed suspension method reduces the impact of the external disturbance and improves the dynamic response speed.


INDEX TERMS Maglev vertical axis wind turbine, magnetic levitation system, adaptive neural network, model predictive control.

I. INTRODUCTION

The wind power generation in low-wind-speed areas is increasingly on the agenda with the development of energy strategies, and low-wind-speed wind power is gradually attracting attention [1], [2], [3]. Unfortunately, low-wind-speed areas often have the disadvantage of frequent changes in wind speed and wind direction; thus the application of vertical axis wind turbines (VAWTs) has received extensive attention. Meanwhile, the unavoidable friction during the rotation of VAWTs essentially reduces the wind energy utilization coefficient. For this reason, it is a good method to introduce a magnetic levitation system (MS) into VAWT [4], [5]. However, the MS is a fragile and weakly damped system, while the VAWT needs some damping to maintain stable operation during the rotation process. Therefore, how to effectively reduce the power consumption, adjust the damping reasonably, and ensure the stability of the system require additional research. For this reason, we propose a novel maglev vertical axis wind turbine (MVAWT) that

adopts the maglev disc motor as the MS and reduces the suspension air gap to 1-2mm, which can effectively control suspension and damping. Therefore, the stable operation of MS is fundamental in MVAWT research.

Nevertheless, due to the characteristics of high nonlinearity, strong coupling, and inherent instability of the MS [6], [7], [8], [9], [10], it is a challenge to achieve stable suspension, especially as the strong disturbance in low-wind-speed areas will bring great challenges to MS. At present, the traditional suspension strategy employs the linear control theory to construct the control law [11], [12], [13], [14], [15], [16]. However, as the operating point often changes and deviates from the operating point, effective control cannot be obtained for this MS. Hence, some intelligent nonlinear control strategies, such as sliding mode control [17], [18], neural network control [19], [20], and fuzzy logic control [21], [22] were introduced into the suspension strategy and achieved corresponding performance improvements. Sun *et al.* [18] proposed an adaptive sliding mode control for MS based on the RBF neural network, but the chattering problem was not well solved. Wai and Lee [19] presented an adaptive neuro-fuzzy control scheme based on the state

The associate editor coordinating the review of this manuscript and approving it for publication was Gerardo Flores .

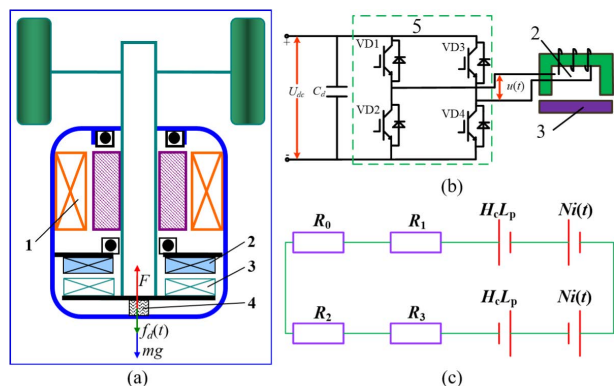


FIGURE 1. Structure sketch of the MVAWT. 1-Permanent Magnet Synchronous Generator, 2-Disc Stator, 3-Disk Rotor, 4-Pressure Sensor, 5- magnetic levitation converter. (a) Structure diagram of maglev vertical axis wind turbine, (b) maglev converter, and (c) the equivalent magnetic circuit model of the hybrid excitation magnet.

observer, but the system convergence speed was not discussed. Su *et al.* [22] presented a fuzzy control scheme with the Takagi-Sugeno model for MS, but the nonlinear model of the MS was simplified and the experiments were not provided to certify it. Although the above-mentioned control methods have better control performance, they are not conducive to engineering implementation because they require large calculation time. In addition, they have no constraints on the input and output states, which makes the robustness of the MS poor and threatens the overall safe operation when the suspension air gap is small. For the MVAWT studied in this paper, reliability, robustness and rapidity are the most important performance indicators. Therefore, model predictive control (MPC) with constraint optimization, simple structure, and multi-objective optimization becomes an ideal suspension strategy, especially as it has been widely employed in the field of power electronics in recent years [23], [24], [25], [26], [27], [28], [29]. In [27], the MPC based on two-level state feedback was designed to ensure the safe and reliable operation of MS. The simulation results showed that this method has better air-gap control ability. In [28], the generalized MPC method based on input and output data was proposed to adjust the parameters of the controller and ensure the system stability while suppressing the vibration caused by the elastic track. In [29], the application of MPC based on a linear parameter-varying model was presented to control the active magnetic bearing subject to input and state constraints. The simulation analysis verified the effectiveness of the proposed control method, but the application of this method required linearization of the magnetic levitation system. However, the suspension strategies based on the MPC in the above studies were all linearized, and the nonlinear characteristic of the MS was ignored, while most of them adopt one-step MPC, which greatly restricts the application of MPC in MS.

To address the above problems and reduce the influence of external disturbance and chattering on the MS, a sliding mode adaptive neural network predictive control method

(SMANNPC) composed of cascade control strategy and an additional auxiliary control is proposed. In the cascade control method, the adaptive neural network predictive control (ANNPC) is applied to the outer loop of suspension pressure and the PID controller is applied in the inner loop of suspension current. The adaptive neural network (ANN) is utilized to approximate the nonlinear MS, which can establish the suspension neural network (SNN) model. Next, the MPC is designed to obtain the optimal control output in the finite time domain, which significantly improved the control performance and realize multi-step prediction. Its global stability with the tracking error converges to zero is proven using the Lyapunov method. Moreover, the auxiliary controller is constructed to compensate for the performance degradation due to model mismatch. Sufficient simulation and experimental results are exhibited to demonstrate better practical performance and anti-disturbance performance. The contribution of this paper lies in three aspects. First, the MVAWT with suspension pressure as suspension objective utilizes the hybrid excitation method and smaller suspension air gap to drastically reduce power consumption. Second, a new suspension control method is proposed, which can ensure that the control system can still obtain satisfactory control performance under harsh conditions. Third, the experimental results show that the proposed method can achieve better control performance than existing methods and show superior robustness.

The remainder of this paper is organized as follows: the dynamic model is established in Section II. In Section III, the suspension control method is presented. Section IV and Section V provide the simulation and experimental results to demonstrate the control performance of the proposed magnetic levitation system. Lastly, the conclusion is presented in Section VI.

II. THE DYNAMIC MODEL OF MS

As shown in Fig. 1(a), the MVAWT mainly contains a permanent magnet synchronous generator, MS, magnetic levitation converter, pressure sensor, etc. The MS consists of a maglev disc motor made up of disc stator and rotor. The disc stator is a hybrid excitation magnet that contains a permanent magnet and electromagnet. As shown in Fig. 1(b), the suspension force can be regulated by adjusting the excitation current of the electromagnet via the magnetic levitation converter based on a four-quadrant H-bridge chopper circuit. The equivalent magnetic circuit model of the hybrid excitation magnet is shown in Fig. 1(c).

The equivalent magnetic circuit model of the hybrid excitation magnet is shown in Fig. 1(c), where R_0 and R_2 denote the air gap reluctance, R_1 and R_3 denote the internal reluctance of the permanent magnet, H_c and L_p are the coercive force and thickness of the permanent magnet, respectively, N is the number of turns of the electromagnet coil, mg is the weight of the rotating body of MVAWT, F is the suspension force generated by the hybrid

excitation magnet, $f_d(t)$ is the external disturbance exerted on the MS.

The total magnetic flux can be expressed as follows

$$\Phi = \frac{2H_c L_p + 2Ni(t)}{R_0 + R_1 + R_2 + R_3} \quad (1)$$

where $i(t)$ is the excitation current of the electromagnet (or called suspension current).

As shown in Fig. 1(c), the structure of the hybrid excitation magnet is symmetric at both ends; thus, $R_0 = R_2 = \delta/(\mu_0 S)$, $R_1 = R_3 = L_p/(\mu_r \mu_0 S)$, in which, μ_0 is the vacuum permeability, μ_r is the relative permeability, S is the magnetic pole area, and δ is the air gap length, i.e. the distance between the disk stator and rotor of the maglev disk motor.

According to the energy balance method, and by substituting (1) into, the suspension force can be obtained as follows

$$F = \frac{dW}{d\delta} = \frac{d}{d\delta} \int_v BHdV = \left(\frac{\Phi}{2S}\right)^2 \frac{S}{\mu_0} = \frac{\mu_0 N^2 S}{4} \left(\frac{H_c L_p/N + i(t)}{L_p/\mu_r + \delta}\right)^2 \quad (2)$$

where, W is the magnetic field energy in volume V , B is the air gap flux density, and H is the air gap magnetic field intensity.

The mechanical equation of MS in the vertical direction is

$$P = mg - \frac{\mu_0 N^2 S}{4} \left(\frac{H_c L_p/N + i(t)}{L_p/\mu_r + \delta}\right)^2 + f_d(t) \quad (3)$$

where, P is the resultant force exerted on the MS in the vertical direction, i.e. the pressure exerted on the pressure sensor by the rotating body of the MVAWT.

The excitation voltage $u(t)$ of the electromagnet is

$$u(t) = Ri(t) + \frac{d\Psi(t)}{dt} = Ri(t) + \frac{d}{dt} (N\Phi) = Ri(t) + \frac{\mu_0 N^2 S}{L_p/\mu_r + \delta} \cdot \frac{di(t)}{dt} \quad (4)$$

where, R and $\Psi(t)$ are the resistance and flux linkage of the electromagnet coil, respectively.

According to (2) - (4), the dynamic model of MS can be obtained as follows

$$\begin{cases} P = mg - \frac{\mu_0 N^2 S}{4} \cdot \left(\frac{H_c L_p/N + i(t)}{L_p/\mu_r + \delta}\right)^2 + f_d(t) \\ u(t) = Ri(t) + \frac{\mu_0 N^2 S}{L_p/\mu_r + \delta} \cdot \frac{di(t)}{dt} \end{cases} \quad (5)$$

III. DESIGN OF SUSPENSION CONTROL STRATEGY

The traditional linear control method cannot suppress external disturbance satisfactorily; hence the MS cannot obtain satisfactory control performance. Therefore, to solve this problem, a suspension control ANNPC is applied to the outer loop of suspension pressure, and the PID controller is applied to the inner loop of suspension current. The output signal of the outer loop of suspension pressure is the input current

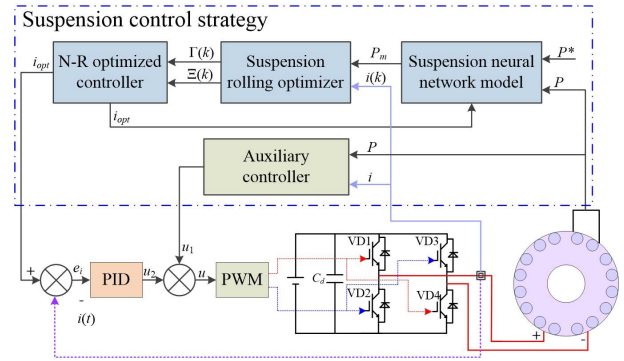


FIGURE 2. Control block of the suspension method of the MS.

reference of the inner loop of suspension current. Moreover, the auxiliary controller is constructed to compensate for performance degradation due to model mismatch.

A. THE AUXILIARY CONTROLLER

The suspension performance can be deteriorated due to model mismatch and uncertain model parameters. Therefore, an auxiliary controller is designed to compensate for the performance degradation problem of ANNPC caused by the model mismatch. According to the dynamic mathematical model of the MS, the derivation of the pressure P can be obtained as follows:

$$\begin{aligned} \dot{P} &= -\frac{\mu_0 N^2 S}{2(L_p/\mu_r + \delta)} (H_c L_p/N + i)\dot{i} + \dot{f}_d \\ &= -\frac{\mu_0 N^2 S (H_c L_p/N + i)}{2(L_p/\mu_r + \delta)} \cdot \left(\frac{L_p/\mu_r + \delta}{\mu_0 N^2 S} (u_p - Ri)\right) + \dot{f}_d \\ &= \frac{(H_c L_p/N + i)Ri}{2} - \frac{H_c L_p/N + i}{2} u_p + \dot{f}_d \end{aligned} \quad (6)$$

Then, the sliding mode surface is designed as $S \triangleq c_1 e_m$, where $c_1 \in R^+$ is the positive gain, and $e_m = P^* - P$ is the tracking error, P^* is the expected suspension pressure value of P , and e_m is ensured to converges 0 when MS is on the sliding mode surface (i. e., $S = 0$).

The derivation of the sliding mode surface S can be calculated as follows:

$$\begin{aligned} \dot{S} &= \dot{P}^* - \dot{P} \\ &= \dot{P}^* - \frac{(H_c L_p/N + i)Ri}{2} + \frac{H_c L_p/N + i}{2} u_p - \dot{f}_d \end{aligned} \quad (7)$$

The exponential reaching law is selected as $\dot{S} = -\nu S - \varpi \tanh(s)$, then, the sliding mode variable structure control law is

$$u_p = \frac{2}{H_c L_p/N + i} (-\dot{P}^* + \dot{f}_d - \nu s - \varpi \tanh(s)) + Ri \quad (8)$$

where ν and $\varpi \in R^+$ represent the constant reaching coefficient and exponential reaching coefficient, respectively. $\tanh(s) = \frac{e^{\iota s} - e^{-\iota s}}{e^{\iota s} + e^{-\iota s}}$ is hyperbolic tangent function that is employed instead of $\text{sgn}(s)$ to reduce chattering, and $\iota \in R^+$ is the positive gain.

In order for the auxiliary controller monitor the system state and make up the system deviation in time, the evaluation

function is selected as $\Lambda = e_m + \dot{e}_m$. Then, the auxiliary control law is designed as follows:

$$u_1 = \gamma u_p \tag{9}$$

where $\dot{\gamma} = -a\Lambda$, a and $\gamma \in R^+$ is the positive control gain.

The auxiliary controller can adaptively detect the system state and make up for system errors caused by model mismatch or large external disturbances in time.

B. THE SNN MODEL

In order to improve the control performance of the MS and avoid linearization when MPC is used as the optimized controller, the ANN is employed to establish the SNN model.

1) CONSTRUCTING THE SNN MODEL

The inputs of the input layer is $x_i(k) = [x_1(k), x_2(k)]^T = [P(k), i(k)]^T$, $i = 1, 2$.

The hidden layer comprises eight neurons; its input $s_j(k)$ and the output $y_j(k)$ of the j -th neuron are

$$\begin{cases} s_j(k) = \sum_{i=1}^2 \omega_{ij}(k)x_i(k) - \theta_j, j = 1, 2, \dots, 8 \\ y_j(k) = f_1(s_j(k)) = f_1\left(\sum_{i=1}^2 \omega_{ij}(k)x_i(k) - \theta_j\right) \end{cases} \tag{10}$$

where $\omega_{ij}(k)$ is the connection weight between the i th input vector and the j th neuron, θ_j is the bias vector of the j th neuron, and $f_1(\cdot) = \tanh(\cdot)$ is the activation function of the output layer.

The output layer involves one neuron; its input $s(k)$ and output $y(k)$ are

$$\begin{cases} s(k) = \sum_{j=1}^8 \omega_j(k)y_j(k) - \xi \\ y(k) = f_2(s(k)) = \sum_{j=1}^8 \omega_j(k)y_j(k) - \xi = P_m(k+1) \end{cases} \tag{11}$$

where $\omega_j(k)$ and ξ denote the connection weight and bias vector of the output layer, respectively, $f_2(\cdot)$ is the activation function of the hidden layer, and $P_m(k+1)$ is the response output value of SNN model.

2) TRAINING THE SNN

The specific steps of using the ANN algorithm to establish the SNN model are as follows:

i) Initialize the connection weights $\omega_{ij}(k)$ and $\omega_j(k)$, and pass the input vector $x_i(k)$ to the input layer successively.

ii) Calculate the output $y_j(k)$ and $y(k)$ by going forward, and compute the error as $e(k) = y(k) - y_r(k) = P_m(k+1) - P(k)$, where $y_r(k)$ is the reference value to $y(k)$.

iii) Adjust the connection weights to $\omega_j(k) = \omega_j(k-1) + \Delta\omega_j(k)$ and $\omega_{ij}(k) = \omega_{ij}(k-1) + \Delta\omega_{ij}(k)$, and return to Step ii) for iterative calculation.

3) CONSTRUCTING THE UPDATE LAW OF CONNECTION WEIGHTS

For the given input $x_i(k)$, the weight vectors $\omega_j(k)$ and $\omega_{ij}(k)$ of the ANN are updated as follows:

$$\begin{cases} \Delta\omega_{ij}(k) = -\omega_{ij}(k-1) + \frac{1}{2x_i(k)} (\theta_j + g_1(q(k))) \\ \Delta\omega_j(k) = \frac{1}{8y_j(k)} \left(y_r(k) + \xi - \sum_{j=1}^8 \omega_j(k-1)y_j(k) \right) \end{cases} \tag{12}$$

where $q(k) = y_r(k)/(8\omega_j(k))$, and $g_1(\cdot) = f_1^{-1}(\cdot)$.

The discrete Lyapunov function is defined as $V(k) = e^2(k)$ to validate that this update law can build the SNN model. The change in the Lyapunov function ΔV is

$$\begin{aligned} \Delta V(k) &= V(k) - V(k-1) \\ &= (y(k) - y_r(k))^2 - e^2(k) \\ &= \left(\sum_{j=1}^8 \omega_j(k)y_j(k) - \xi - y_r(k) \right)^2 - e^2(k-1) \\ &= \left(\sum_{j=1}^8 (\omega_j(k-1) + \Delta\omega_j(k))y_j(k) - \xi - y_r(k) \right)^2 - e^2(k-1) \\ &= \left(\sum_{j=1}^8 \omega_j(k-1)y_j(k) + \Delta\omega_j(k)y_j(k) - \xi - y_r(k) \right)^2 - e^2(k-1) \end{aligned} \tag{13}$$

Then,

$$\begin{aligned} e(k) &= y(k) - y_r(k) \\ &= \sum_{j=1}^8 \omega_j(k)y_j(k) - y_r(k) \\ &= \sum_{j=1}^8 \omega_j(k)f_1\left(\sum_{i=1}^2 (\omega_{ij}(k-1) + \Delta\omega_{ij}(k))x_i(k) - \theta_j\right) - y_r(k) \\ &= \sum_{j=1}^8 f_1\left(\sum_{i=1}^2 (\omega_{ij}(k-1)x_i(k) + \Delta\omega_{ij}(k)x_i(k)) - \theta_j\right) \cdot \omega_j(k) - y_r(k) \end{aligned} \tag{14}$$

Substituting (12) into (14), the error e can be obtained as

$$\begin{aligned} e(k) &= \sum_{j=1}^8 \omega_j(k) \cdot \\ &= f_1\left(\sum_{i=1}^2 (\omega_{ij}(k-1)x_i(k) + \Delta\omega_{ij}(k)x_i(k)) - \theta_j\right) - y_r(k) \end{aligned}$$

$$\begin{aligned}
 &= \sum_{j=1}^8 \omega_j(k) f_1 \left(\sum_{i=1}^2 \frac{1}{2} (\theta_j + g_1(q_1(k))) - \theta_j \right) - y_r(k) \\
 &= 0 \tag{15}
 \end{aligned}$$

From (15) and (13), there is $\Delta V(k) = -e^2(k-1) < 0$.

Remark 1: By constructing the above updated law, the error between reference output $y_r(k)$ and actual output $y(k)$ can quickly converge to 0.

To prevent the singularities caused by the zero value of the $q_j(k)$, $x_i(k)$ and $\omega_j(k)$, the weight update laws $\Delta\omega_j(k)$ and $\Delta\omega_{ij}(k)$ can be modified as follows

$$\Delta\omega_j(k) = \frac{1}{8(y_j(k) + \vartheta_1)} \left(y_r(k) + \xi - \sum_{j=1}^8 \omega_j(k-1)y_j(k) \right)$$

$$\Delta\omega_{ij}(k) = -\omega_{ij}(k-1) + \frac{1}{2(x_i(k) + \vartheta_2)} (\theta_j + g_1(q(k)))$$

where

$$q(k) = \frac{1}{8(\omega_j(k) + \vartheta_3)} y_r(k)$$

The values of ϑ_1 , ϑ_2 , and ϑ_3 are the small positive numbers.

C. THE ADAPTIVE NEURAL NETWORK PREDICTIVE CONTROLLER

The role of the optimizer is to obtain the optimal control output, i.e. the reference suspension current i_{opt} , through the rolling optimization of suspension cost function $J(k)$ with the following constrained finite-horizon optimization, which is selected as follows:

$$\begin{aligned}
 J(k) &= \alpha \sum_{l=1}^{N_p} (P^*(k+l) - P_m(k+l))^2 + \lambda \sum_{l=1}^{N_u} (i(k+l-1) \\
 &\quad - i(k+l-2))^2 \tag{16}
 \end{aligned}$$

subject to

$$\begin{aligned}
 i_{min} &\leq i(k) \leq i_{max} \\
 P_{min} &\leq P_m(k) \leq P_{max} \\
 \Delta i_{min} &\leq \Delta i(k) \leq \Delta i_{max}
 \end{aligned}$$

$$P^*(k+N_p+j) - P_m(k+N_p+j) = 0, \quad j \geq 1$$

where $P^*(k) = [P^*(k+1), P^*(k+1), \dots, P^*(k+N_p)]^T$ is the vector of reference trajectory of MS, $P_m(k) = [P_m(k+1), P_m(k+1), \dots, P_m(k+N_p)]^T$ is the vector of response output of SNN model, and $\Delta i(k) = i(k) - i(k-1) = [\Delta i(k), \Delta i(k+1), \dots, \Delta i(k+N_u-1)]^T$ is the future control increment. α and λ are the pressure weighting factor and the current weighting factor, respectively; N_p is the prediction horizon, N_u is the control horizon ($N_p = N_u = d$), and d means the prediction steps.

To obtain and maintain the actual optimal control and reduce the number of iterations required to achieve the optimum, the Newton-Raphson method is utilized as the optimized controller, and the predictive value of the suspension current at the $(k+1)$ -th moment is

$$i(k+1) = i(k) - [\Xi(k)]^{-1} \Gamma(k) \tag{17}$$

where $\Gamma(k)$ and $\Xi(k)$ are the Jacobian matrix and Hessian matrix, respectively, and $i(k+1)$ is just the suspension current reference $i_{opt}(k)$.

By calculating the current deviation $e_i = i_{opt} - i$, the control law of suspension current inner loop can be obtained as follows:

$$u_2 = K_p e_i + K_i \int e_i + K_d \dot{e}_i \tag{18}$$

where, K_p , K_i and K_d are the proportional coefficient, integral coefficient and differential coefficient, respectively.

By taking the first-order and second-order derivatives of (11), respectively, $\Gamma(k)$ and $\Xi(k)$ can be obtained as follows:

$$\Gamma(k) = \left[\frac{\partial J}{\partial i(k)}, \frac{\partial J}{\partial i(k+1)}, \dots, \frac{\partial J}{\partial i(k+d-1)} \right]^T \tag{19}$$

$$\Xi(k) = \begin{bmatrix} \frac{\partial^2 J}{\partial i(k)^2} & \dots & \frac{\partial^2 J}{\partial i(k)\partial i(k+d-1)} \\ \frac{\partial^2 J}{\partial i(k+1)\partial i(k)} & \dots & \frac{\partial^2 J}{\partial i(k+1)\partial i(k+d-1)} \\ \vdots & \ddots & \vdots \\ \frac{\partial^2 J}{\partial i(k+d-1)\partial i(k)} & \dots & \frac{\partial^2 J}{\partial i(k+d-1)^2} \end{bmatrix} \tag{20}$$

The proposed SMANNPC consisted of an auxiliary controller and an ANNPC. Hence, according to Equations (9) and (18), the control law of SMANNPC can be obtained as follows:

$$\begin{aligned}
 u &= u_1 + u_2 \\
 &= \gamma \left(\frac{2(L_p/\mu_r + \delta)}{H_c L_p / N + i} (-\dot{P}^* + \dot{f}_d - v_s - \varpi \tanh(s)) + Ri \right) \\
 &\quad + K_p e_i + K_i \int e_i + K_d \dot{e}_i
 \end{aligned}$$

D. STABILITY ANALYSIS

The stability performance is essential to the successful application of SMANNPC [30-31]. In this section, the stability of SMANNPC is intensively investigated by employing terminal constraints of MPC.

Theorem: Consider the constrained finite-horizon optimal control problem represented by Equation(16), and the control law designed as Equation(17); then, the asymptotic stability of the proposed SMANNPC can be guaranteed.

Proof: If $i(0)$ is feasible for $P^*(0)$, then $i(0)$ is feasible at all time-steps $k \geq 0$ (recursive feasibility).

1) By taking Th. 3 into account [32], it is easy to see that if $i(k-1)$ satisfies Equations(16) and (17) for $P^*(k-1)$, then $i(k)$ satisfies Equations(16) and (17) for $P^*(k)$. As $i(0)$ is feasible at $k=0$, it can be proven recursively that $i(k)$ is feasible for all time steps $k \geq 0$.

2) The $i(k) = [i(k), i(k+1), \dots, i(k+N_u-1)]^T$ is postulated as the optimal control found by the optimization procedure at the k -th moment. Now, let us present the suboptimal control $i_s(k+1)$ assumed at the $(k+1)$ -th moment.

$$i_s(k+1) = \underbrace{[i(k+1), \dots, i(k+N_u-1)]}_{N_u-1}^T, i(k+N_u-1) \tag{21}$$

TABLE 1. Simulation parameters of MS.

Parameter	Value	Parameter	Value
g (m/s ²)	9.8	δ (mm)	2
m (kg)	130	R (Ω)	0.7
S (m ²)	1.2×10^{-2}	μ_0 (N/A ²)	$4\pi \times 10^{-7}$

The control sequence $i_s(k+1)$ is obtained on the basis of the control at time k . Hence, for the suboptimal control $i_s(k+1)$, the cost function can be defined as follows:

$$J_s(k+1) = \alpha \sum_{l=2}^{N_p+1} (P^*(k+l) - P_m(k+l))^2 + \lambda \sum_{l=2}^{N_u} \Delta i(k+l-1)^2 \quad (22)$$

Then, the difference in cost function $J_s(k+1)$ and $J(k)$ can be calculated as follows

$$J_s(k+1) - J(k) = \alpha [(P^*(k+N_p+1) - P_m(k+N_p+1))^2 - (P^*(k+1) - P_m(k+1))^2] - \lambda \Delta i(k)^2$$

Additionally, if $i(k+1)$ is the optimal solution at time $(k+1)$, then, when $i_s(k+1)$ is the suboptimal, $J(k+1) \leq J_s(k+1)$, we have

$$J(k+1) - J(k) \leq J_s(k+1) - J_s(k) \leq 0 \quad (23)$$

Therefore, by taking (23), **Theorem** can be proven.

Remark 2: As the proposed SMANNPC requires solving a constrained nonlinear optimization problem, the problems of feasibility and stability are extremely important. The feasibility and stability of the SMANNPC are proven by **Theorem**. The tracking performance and control accuracy of MS will be improved as the number of prediction steps of SMANNPC increases. However, it will increase the time consumption of MS and cause the dynamic response performance to deteriorate. Therefore, in order to ensure the overall performance of MS, two prediction steps are selected and compared with the traditional one-step prediction.

IV. SIMULATION ANALYSIS

A simulation platform was built to verify the control performance of the proposed control method. The ANNPC and PID controller were applied to the outer loop of suspension pressure and the inner loop of suspension current of the SMANNPC-PID, respectively, while the auxiliary controller output was superimposed on the cascade control output. The SMANNPC-PID was compared with ANNPC2-PID, ANNPC1-PID, and PID-PID in this simulation experiment. The parameters of the MS are listed in Table 1; among them the mass m of the rotating body of MVAWT is 130kg, the suspension force generated by the permanent magnet of the hybrid excitation magnet is 1014N, and the initial pressure is about 260N. The expected suspension pressure of the MS is set to 50N. The switching frequency of the MS is 10kHz.

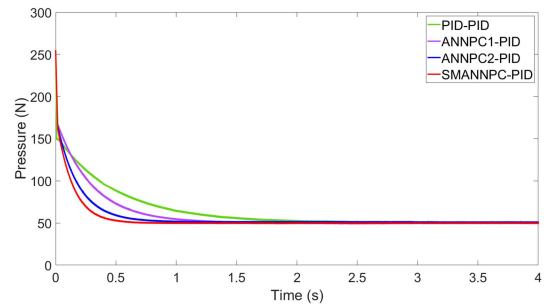


FIGURE 3. Suspension pressure under non-disturbance condition.

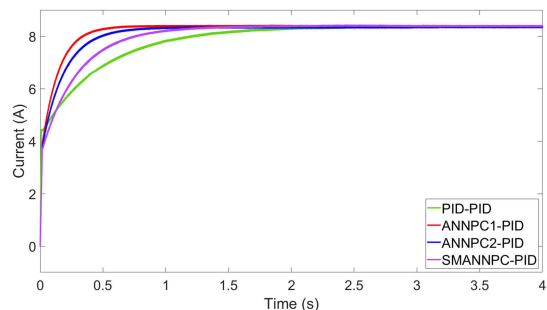


FIGURE 4. Suspension current under non-disturbance condition.

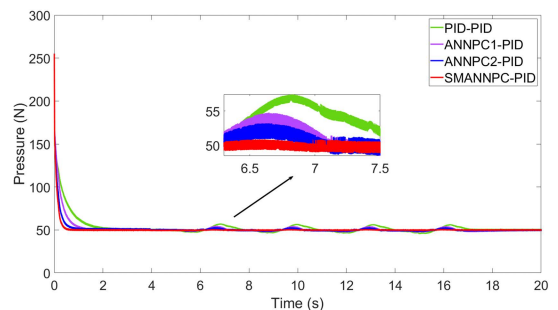


FIGURE 5. Suspension pressure under disturbance $f_d(t)$.

The control parameters of the proposed method can be divided into two, one is the parameters for the ANNPC and PID control, and the other is the parameters for auxiliary controller. After sufficient tuning, the parameters of ANNPC and PID are obtained:

$\omega_{ij}=[0.90, 0.88; 0.56, 0.60; 0.48, 0.06; 0.59, 0.32; 0.23, 0.79; 0.52, 0.71; 0.65, 0.05; 0.11, 1.1], \theta_j=[-0.2; 0.23; 0.75; 0.97; 0.3; -0.72; -1.1; 0.22]; \omega_j=[-0.02, 0.31, 0.28, -0.11, 0.26, -0.68, 0.44, 0.19], \xi=-1.06; \vartheta=0.0001; \alpha=\lambda=1; K_p=1000, K_i=10, K_d=5.$

The other are auxiliary control parameters, which are selected as:

$c_1=10, v=5, \varpi=10, \iota=1, a=0.5.$

A. SIMULATION FOR DYNAMIC RESPONSE PERFORMANCE

The control effects of SMANNPC-PID, ANNPC2-PID, ANNPC1-PID, and PID-PID were compared to examine the

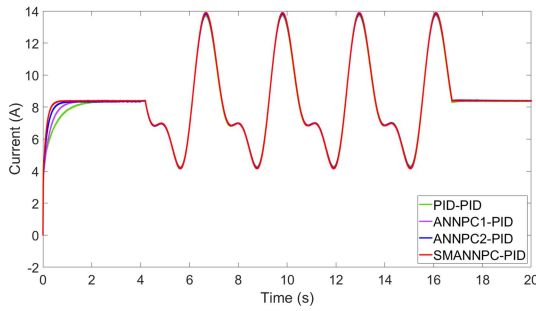


FIGURE 6. Suspension current under disturbance $f_d(t)$.

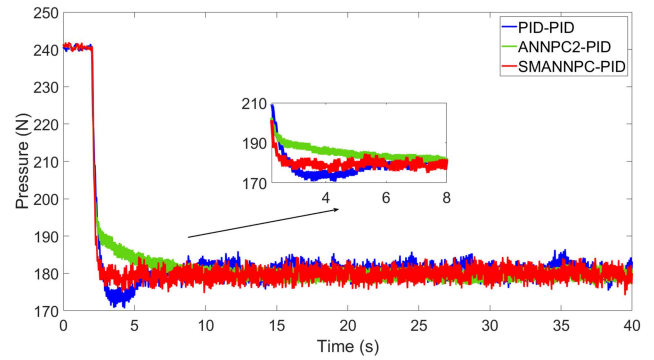


FIGURE 8. Suspension pressure under non-disturbance condition.

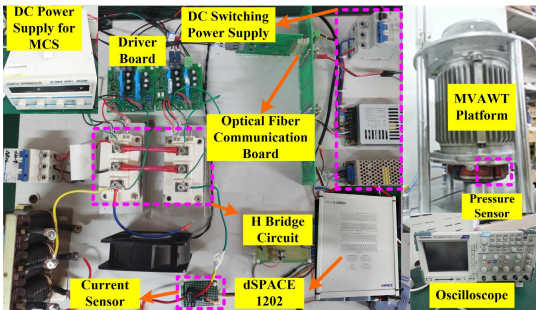


FIGURE 7. The experimental platform of MVAWT.

dynamic response performance of the proposed suspension strategy.

It is shown in Fig. 3 that the system with the PID-PID had a settling time of more than 3s. The system with the ANNPC1-PID needed more than 2s and showed vibrations in the results. The system with the ANNPC2-PID had a settling time of more than 1.3s, and the system with the proposed SMANNPC-PID had a settling time of less than 0.6s. The static error in the SMANNPC-PID was smaller than that in the ANNPC2-PID. Furthermore, compared with ANNPC1-PID, ANNPC2-PID, and PID-PID, the dynamic response speed of SMANNPC-PID was increased and the suspension current was much smoother. This shows that the proposed control method has stronger control capability and faster tracking performance.

B. SIMULATION FOR ANTI-DISTURBANCE PERFORMANCE

In order to verify the robustness and anti-disturbance capability of the proposed suspension strategy, the nonlinear periodic disturbance $f_d(t) = 100\sin(2t - 100) + 50\sin(4t - 50)$ was added to MS at 4s and removed at 17s. The simulation results under this disturbance $f_d(t)$ are shown in Figs. 5-6.

As shown in Fig. 5, the suspension pressure of PID-PID changed constantly with the variation of external disturbance, which had a maximum static error of more than 8N. The suspension pressure fluctuation of ANNPC1-PID exceeded 5N and that of ANNPC2-PID was more than 3N. Meanwhile, the suspension pressure fluctuation of SMANNPC-PID was less than 1N. Moreover, when the external disturbance was removed, the static error of PID-PID still existed, and ANNPC1-PID had a suspension pressure

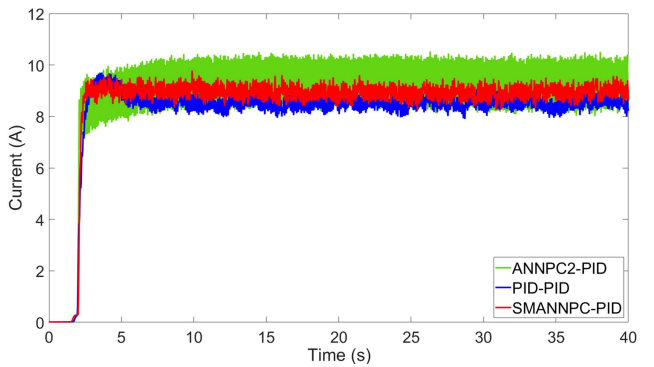


FIGURE 9. Suspension current under non-disturbance condition.

fluctuation of more than 5N. The suspension pressure fluctuation of ANNPC2-PID was more than 3N, while that of ANNPC2-PID was less than 1N and could be restored to its steady state within 0.2s. As shown in Fig. 6, the SMANNPC-PID had the maximum suspension current fluctuation of 10A, while the PID-PID had the minimum suspension current fluctuation of 9.5A. Therefore, when MS is subjected to external disturbance, the SMANNPC-PID can better restrain the disturbance and improve the robustness of the MS.

V. EXPERIMENTAL RESULTS

In order to further examine the practical performance of the proposed control method, a physical prototype of the 1kW MVAWT was developed, and the experimental platform shown in Fig. 7 was built. On this basis, this paper adopted dSPACE 1202 and the maglev converter as the suspension controller. The expected suspension pressure was set to 180N with an initial value of 240N, the control frequency was 10kHz, and the supply voltage was 36V. Two sets of experiments were carried out to validate the tracking performance and the anti-disturbance capability.

For the experiments, the control gains and parameters are carefully determined as follows:

$$\omega_{ij} = [0.90, 0.88; 0.56, 0.60; 0.48, 0.06; 0.59, 0.32; 0.23, 0.79; 0.52, 0.71; 0.65, 0.05; 0.11, 1.1], \theta_j = [-0.2; 0.23; 0.75; 0.97; 0.3; -0.72; -1.1; 0.22]; \omega_j = [-0.02, 0.31, 0.28, -0.11, 0.26, -0.68, 0.44, 0.19], \xi = -1.06; \vartheta = 0.0001; \alpha = \lambda = 1;$$

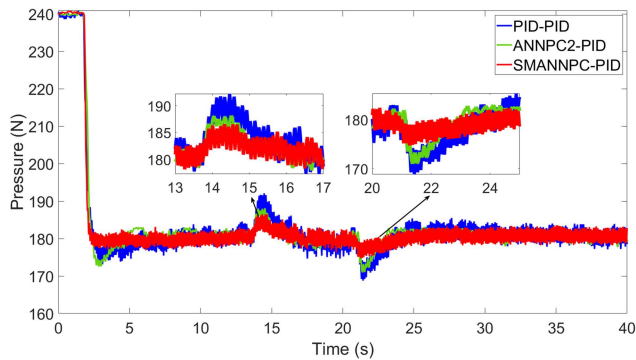


FIGURE 10. Suspension pressure under disturbance $f_d(t)$ condition.

$c_1 = 10, v = 5, \varpi = 10, \iota = 1, a = 0.5; K_p = 1000, K_i = 10, K_d = 5.$

A. EXPERIMENT FOR DYNAMIC RESPONSE PERFORMANCE

An experiment was employed to examine the dynamic response performance of the SMANNPC-PID, ANNPC2-PID, and PID-PID. The initial position of the suspension pressure was 240N, and, from the time $t = 2s$, the corresponding control laws were utilized to drive the MS to the reference position of 180N. In the PID-PID, the PID control parameters of outer loop of the suspension pressure were 100, 50, and 100, respectively. And the PID control parameters of inner loop of the suspension current were 14, 5, and 10, respectively. The experiment results are shown in Figs. 8-9.

It can be seen from Fig. 8 that the system with the SMANNPC-PID method had a settling time of less than 0.5s without obvious suspension pressure fluctuation. The system with the ANNPC2-PID method had a settling time of more than 7s and the suspension pressure fluctuation is less than 7N, while, for that with PID-PID, the settling time was more than 4s and the suspension pressure fluctuation was more than 10N. Compared with PID-PID and ANNPC2-PID, the SMANNPC-PID could reach a stable state in the shortest time and suppress overshoot well due to the synergy between the auxiliary controller and ANNPC. Moreover, it is shown in Fig. 9 that the system with the PID-PID method had a suspension current fluctuation of more than 1.5A and a current ripple of more than 1A. Although the suspension current fluctuation of ANNPC2-PID was less than 1A, it had a current ripple of more than 2A. In contrast, the system with the SMANNPC-PID had no obvious suspension current fluctuation and had a current ripple of less than 0.7A. Compared with ANNPC2-PID, the SMANNPC-PID can effectively reduce the suspension current fluctuation of the MS while quickly reaching the desired position, which can improve the working efficiency of the system. These experimental results demonstrate that the proposed control method had faster dynamic response capability and better tracking performance.

B. EXPERIMENT FOR ANTI-DISTURBANCE PERFORMANCE

An experiment was utilized to examine the anti-disturbance performance of the three control methods. A nonlinear

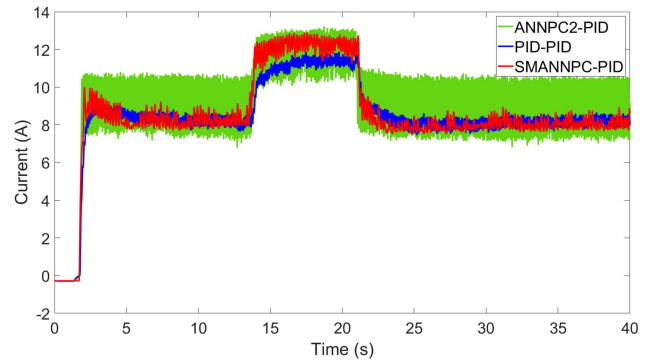


FIGURE 11. Suspension current under disturbance $f_d(t)$ condition.

TABLE 2. Simulation parameters of MS.

Experiment		SMANNPC-PID	ANNPC2-PID	PID-PID
Case 1: normal	Settling Time	<0.5s	>7s	>4s
	Pressure Fluctuation	<1N	<7N	>10N
	Current Fluctuation	<0.7A	<1A	>1.5A
Case 2: disturbance	Settling Time	<2s	>3s	>5s
	Pressure Fluctuation	<6N	>8N	>10N

external disturbance with amplitude of 30N was added at 14s and removed at 21s. The experimental results are shown in Figs. 10-11.

As shown in Fig. 10, when external disturbance was added, the system with the SMANNPC-PID method had a suspension pressure fluctuation of less than 6N, and the settling time was less than 2s. The suspension pressure fluctuation of the ANNPC2-PID method exceeded 8N with a settling time of more than 3s. In contrast, the PID-PID method had a suspension pressure fluctuation of more than 10N and required a settling time of more than 5s. Although PID-PID can suppress the external disturbance, it had large suspension pressure fluctuation and takes more time to restore the original equilibrium position. In addition, both ANNPC2-PID and SMANNPC-PID could restore the equilibrium state in a shorter time, but SMANNPC-PID had stronger anti-disturbance ability and faster settling time. It is clear in Fig. 11 that, compared with ANNPC2-PID and PID-PID, the suspension current of SMANNPC-PID could react quickly in a short time when external disturbance was applied to the MS.

The ANNPC2-PID could use the ANN to establish an accurate SNN model, when the system deviated from the equilibrium position, it could reach the new equilibrium position quickly. However, the fast response of the system led to a large suspension current ripple, which may cause chattering in the system and will degrade system performance. While in SMANNPC-PID, due to the additional compensation effect of the auxiliary controller, the system could reach the steady state in a shorter time without obvious

suspension pressure fluctuation and suspension current ripple. Since the integral term was added and the continuous hyperbolic tangent function was used instead of the sign function as the switching control law in the auxiliary controller of SMANNPC-PID, when the external disturbance was added to this system, the proposed SMANNPC-PID could quickly suppress the external disturbance and reduce the suspension current ripple.

The numerical values are summarized in a statistical table in Table 2. By summarizing the numerical values in Table 2, it can be seen that the presented suspension control method can achieve better control performance and better disturbance rejection capability under the condition of smooth control current and external disturbance.

VI. CONCLUSION

This paper studied the MS in MVAWT. To improve the suspension control performance of MS, the SMANNPC was presented using an auxiliary controller, an adaptive neural network, and a model predictive control to handle external disturbance and unmatched uncertainties in the system. The stability of the proposed control method was proven by the Lyapunov theorem. Compared with the PID controller and ANNPC, the simulation and experimental results show that the proposed nonlinear robust controller had a non-overshooting, robust, fast dynamic response and could effectively reduce the impact of external disturbance on the system. Furthermore, it could solve the problems of external disturbance and parameter perturbation with a faster adjustment speed while meeting the control quality requirements of MVAWT.

In the nonlinear systems with external disturbance and parameter perturbation, the SMANNPC can adaptively adjust the system parameters, showing better control performance. However, when this control method is applied to other nonlinear systems, the control parameters need to be readjusted according to the actual working conditions, which will take more time and reduce work efficiency. Next, we will study SMANNPC further, so that it can be easily generalized to other nonlinear systems.

REFERENCES

- [1] E. Mohammadi, R. Fadaeinedjad, H. R. Naji, and G. Moschopoulos, "Investigation of horizontal and vertical wind shear effects using a wind turbine emulator," *IEEE Trans. Sustain. Energy*, vol. 10, no. 3, pp. 1206–1216, Jul. 2019.
- [2] M. A. Soliman, H. M. Hasanien, H. Z. Azazi, E. E. El-Kholy, and S. A. Mahmoud, "An adaptive fuzzy logic control strategy for performance enhancement of a grid-connected PMSG-based wind turbine," *IEEE Trans. Ind. Informat.*, vol. 15, no. 6, pp. 3163–3173, Jun. 2019.
- [3] S. Hu, G. Zhu, and Y. Kang, "Modeling and coordinated control design for brushless doubly-fed induction generator-based wind turbine to withstand grid voltage unbalance," *IEEE Access*, vol. 9, pp. 63331–63344, 2021.
- [4] X. Chu, "Two degrees of freedom cooperative suspension control for maglev wind yaw system," *IEEE/ASME Trans. Mechatronics*, vol. 27, no. 3, pp. 1425–1435, Jun. 2022.
- [5] X. Chu, "Two-terminal suspension adaptive control with synchronous compensation for maglev wind turbine yaw system," *IEEE Trans. Ind. Electron.*, vol. 69, no. 10, pp. 10530–10540, Oct. 2022.
- [6] F. Xu, X. Lu, T. Zheng, and X. Xu, "Motion control of a magnetic levitation actuator based on a wrench model considering yaw angle," *IEEE Trans. Ind. Electron.*, vol. 67, no. 10, pp. 8545–8554, Oct. 2020.
- [7] M.-Y. Chen, C.-F. Tsai, and L.-C. Fu, "A novel design and control to improve positioning precision and robustness for a planar maglev system," *IEEE Trans. Ind. Electron.*, vol. 66, no. 6, pp. 4860–4869, Jun. 2019.
- [8] Y. Sun, H. Qiang, J. Xu, and G. Lin, "Internet of Things-based online condition monitor and improved adaptive fuzzy control for a medium-low-speed maglev train system," *IEEE Trans. Ind. Informat.*, vol. 16, no. 4, pp. 2629–2639, Apr. 2020.
- [9] S. Mirić, P. Küttel, A. Tüysüz, and J. W. Kolar, "Design and experimental analysis of a new magnetically levitated tubular linear actuator," *IEEE Trans. Ind. Electron.*, vol. 66, no. 6, pp. 4816–4825, Jun. 2019.
- [10] C. Zhao, K. Oka, F. Sun, A. Harada, J. Jin, and M. Zhang, "Design of zero-power control strategy with resisting tilt of hybrid magnetic levitation system," *IEEE Trans. Ind. Electron.*, vol. 69, no. 11, pp. 11394–11402, Nov. 2022.
- [11] D. Zhou, Q. Yang, L. Wang, and J. Li, "Stability and control of maglev vehicle-girder coupled system considering torsional vibration of the girder," *ISA Trans.*, vol. 111, pp. 309–322, May 2021.
- [12] Q. Ouyang, K. Fan, Y. Liu, and N. Li, "Adaptive LADRC parameter optimization in magnetic levitation," *IEEE Access*, vol. 9, pp. 36791–36801, 2021.
- [13] B. Xin, Y. Wang, W. Xue, T. Cai, Z. Fan, J. Zhan, and J. Chen, "Evolution of controllers under a generalized structure encoding/decoding scheme with application to magnetic levitation system," *IEEE Trans. Ind. Electron.*, vol. 69, no. 9, pp. 9655–9666, Sep. 2022.
- [14] X. D. Zhang, M. Mehrtash, and M. B. Khamesee, "Dual-axial motion control of a magnetic levitation system using hall-effect sensors," *IEEE-ASME Trans. Mechatronics*, vol. 21, no. 2, pp. 1129–1139, Apr. 2016.
- [15] S. K. Kim and C. K. Ahn, "Variable cut-off frequency algorithm-based nonlinear position controller for magnetic levitation system applications," *IEEE Trans. Syst., Man, Cybern., Syst.*, vol. 51, no. 7, pp. 4599–4605, Jul. 2021.
- [16] Y. Sun, J. Xu, H. Y. Qiang, and G. B. Lin, "Adaptive neural-fuzzy robust position control scheme for maglev train systems with experimental verification," *IEEE Trans. Ind. Electron.*, vol. 66, no. 11, pp. 8589–8599, Nov. 2019.
- [17] H. S. Zad, T. I. Khan, and I. Lazoglu, "Design and adaptive sliding-mode control of hybrid magnetic bearings," *IEEE Trans. Ind. Electron.*, vol. 65, no. 3, pp. 2537–2547, Mar. 2017.
- [18] Y. Sun, J. Xu, H. Qiang, C. Chen, and G. Lin, "Adaptive sliding mode control of maglev system based on RBF neural network minimum parameter learning method," *Measurement*, vol. 141, pp. 217–226, Jul. 2019.
- [19] R.-J. Wai and J.-D. Lee, "Robust levitation control for linear maglev rail system using fuzzy neural network," *IEEE Trans. Control Syst. Technol.*, vol. 17, no. 1, pp. 4–14, Jan. 2009.
- [20] Y. Sun, J. Xu, G. Lin, W. Ji, and L. Wang, "RBF neural network-based supervisor control for maglev vehicles on an elastic track with network time delay," *IEEE Trans. Ind. Informat.*, vol. 18, no. 1, pp. 509–519, Jan. 2022.
- [21] L. Yipeng, L. Jie, Z. Fengge, and Z. Ming, "Fuzzy sliding mode control of magnetic levitation system of controllable excitation linear synchronous motor," *IEEE Trans. Ind. Appl.*, vol. 56, no. 5, pp. 5585–5592, Sep. 2020.
- [22] X. Su, X. Yang, P. Shi, and L. Wu, "Fuzzy control of nonlinear electro-magnetic suspension systems," *Mechatronics*, vol. 24, no. 4, pp. 328–335, Jun. 2014.
- [23] M. Cetin and S. Iplikci, "A novel auto-tuning PID control mechanism for nonlinear systems," *ISA Trans.*, vol. 58, pp. 292–308, Sep. 2015.
- [24] X. Liu, D. Wang, and Z. Peng, "Cascade-free fuzzy finite-control-set model predictive control for nested neutral point-clamped converters with low switching frequency," *IEEE Trans. Control Syst. Technol.*, vol. 27, no. 5, pp. 2237–2244, Sep. 2019.
- [25] N. Jabbour and C. Mademlis, "Online parameters estimation and auto-tuning of a discrete-time model predictive speed controller for induction motor drives," *IEEE Trans. Power Electron.*, vol. 34, no. 2, pp. 1548–1559, Feb. 2018.
- [26] J. Theunissen, A. Sornioti, P. Gruber, S. Fallah, M. Ricco, M. Kvasnica, and M. Dhaens, "Regionless explicit model predictive control of active suspension systems with preview," *IEEE Trans. Ind. Electron.*, vol. 67, no. 6, pp. 4877–4888, Jun. 2020.
- [27] Z. Zhang, Y. Zhou, and X. Tao, "Model predictive control of a magnetic levitation system using two-level state feedback," *Meas. Control*, vol. 53, nos. 5–6, pp. 962–970, May 2020.

- [28] Y. Y. Wang and J. Li, "Levitation system controller design based on the implicit general predictive control algorithm," *Appl. Mech. Mater.*, vols. 444–445, pp. 806–811, Oct. 2013.
- [29] A. Morsi, H. S. Abbas, S. M. Ahmed, and A. M. Mohamed, "Model predictive control based on linear parameter-varying models of active magnetic bearing systems," *IEEE Access*, vol. 9, pp. 23633–23647, 2021.
- [30] Z. Fan, T. Chan, Y. Yang, and J. Jang, "Backpropagation with N -D vector-valued neurons using arbitrary bilinear products," *IEEE Trans. Neural Netw. Learn. Syst.*, vol. 31, no. 7, pp. 2638–2652, Jul. 2020.
- [31] T. Shen and I. R. Petersen, "Linear threshold discrete-time recurrent neural networks: Stability and globally attractive sets," *IEEE Trans. Autom. Control*, vol. 61, no. 9, pp. 2650–2656, Sep. 2016.
- [32] H.-G. Han, L. Zhang, Y. Hou, and J.-F. Qiao, "Nonlinear model predictive control based on a self-organizing recurrent neural network," *IEEE Trans. Neural Netw. Learn. Syst.*, vol. 27, no. 2, pp. 402–415, Feb. 2016.



YANG ZHANG received the B.S. degree in automation from Qufu Normal University, Rizhao, China, in June 2019, where she is currently pursuing the M.S. degree in control science and engineering with the College of Engineering.

Her research interests include containment control, event-triggered control, and nonlinear multiagent systems control.



YIXI CHEN was born in 1997. He received the B.S. degree in electrical engineering and its automation from Qufu Normal University, Rizhao, China, in June 2019, where he is currently pursuing the M.S. degree in control science and engineering with the College of Engineering.

His current research interests include renewable power generation, power electronics, and magnetic levitation technology.



BIN CAI received the Ph.D. degree in electrical engineering from Xi'an Jiaotong University, Xi'an, China. He is currently a Professor with the College of Engineering, Qufu Normal University, Rizhao, China. His research interests include wind power generation and the applications of artificial intelligent in the renewable energy control fields, power electronics and HVDC-flexible transmission technology.

...